Applied Physics Letters ARTICLE pubs.aip.org/aip/apl

Enhanced thermal performance of AlN/GaN/AlN XHEMTs on bulk AlN by suppression of phonon-boundary scattering

Cite as: Appl. Phys. Lett. **127**, 233505 (2025); doi: 10.1063/5.0305053
Submitted: 2 October 2025 · Accepted: 25 November 2025 ·
Published Online: 12 December 2025

View Online Export Citation CrossMark

Yiwen Song,[1] Eungkyun Kim,[2,3] Jimy Encomendero,[2] Seokjun Kim,[1] Daniel C. Shoemaker,[1] Yu-Hsin Chen,[4] Debdeep Jena,[2,3,4] Huili Grace Xing,[2,3,4,a)] and Sukwon Choi[1,a)]

AFFILIATIONS

[1]Department of Mechanical Engineering, The Pennsylvania State University, University Park, Pennsylvania 16082, USA
[2]School of Electrical and Computer Engineering, Cornell University, Ithaca, New York 14853, USA
[3]Kavli Institute at Cornell for Nanoscale Science, Cornell University, Ithaca, New York 14853, USA
[4]Department of Materials Science and Engineering, Cornell University, Ithaca, New York 14853, USA

Note: This paper is part of the Special Topic on Frontiers in Nitride Semiconductors Research.
[a)]**Authors to whom correspondence should be addressed:** grace.xing@cornell.edu and sukwon.choi@psu.edu

ABSTRACT

AlN/GaN/AlN high electron mobility transistors (HEMTs) have demonstrated exceptional potential for surpassing the electrical limitations of conventional AlGaN/GaN HEMTs. This study investigates the thermal performance of two types of AlN/GaN/AlN HEMTs with homoepitaxial AlN buffer layers grown on AlN substrates: an AlN/GaN/AlN single-crystal HEMT (AlN XHEMT) featuring a pseudomorphic/thin GaN channel and a conventional structure with a relaxed/thick GaN channel. Frequency- and time-domain thermoreflectance measurements reveal bulk-like thermal conductivity in the homoepitaxial AlN buffer layer, with negligible thermal boundary resistance at the AlN buffer/substrate interface. Consequently, Raman thermometry demonstrates that the AlN XHEMT with a thin (~20 nm) pseudomorphically strained GaN channel exhibits better thermal performance than identical HEMT layer structures grown on a 4H-SiC substrate, despite 4H-SiC possessing a higher thermal conductivity. In addition, the AlN XHEMT exhibits a 22% lower channel temperature under 14 W/mm power density than the AlN/GaN/AlN-on-AlN HEMT that employs a thick (275 nm) relaxed GaN channel. These findings highlight that AlN XHEMTs offer not only electrical but also thermal advantages for high-power and high-frequency applications.

Gallium nitride (GaN)-based devices excel in high-frequency and high-power applications, notably as radio frequency (RF) power amplifiers. These amplifiers are essential parts for fifth-generation (5G) cell towers, satellite communications, military radars, and electronic warfare systems.[1] Conventional AlGaN/GaN high electron mobility transistors (HEMTs) utilize a polarization-induced two-dimensional electron gas (2DEG) formed near the AlGaN/GaN heterointerface, enabling high carrier mobility.[2] Despite significant advancements in AlGaN/GaN HEMTs, gate leakage and current collapse persist as challenges for millimeter-wave high-frequency applications.[3–5] The AlGaN barrier in AlGaN/GaN HEMTs can exhibit gate leakage due to the low Schottky barrier height and material defect-induced trap states that result in trap-assisted tunneling and Poole–Frenkel emission.[6] Additionally, the slow time constants of these trap states capture electrons, leading to current collapse at high operating frequencies.[7] Moreover, as the gate length is scaled down, the AlGaN barrier thickness must be reduced to minimize gate-source capacitance to ensure sufficient transconductance for high gain and speed in millimeter-wave applications. However, this thinner barrier exacerbates gate leakage through enhanced Fowler–Nordheim tunneling and larger field-induced Poole–Frenkel emission, compromising device reliability and efficiency.[8]

To address the limitations associated with the AlGaN barrier, AlN/GaN/AlN high electron mobility transistors (HEMTs) were recently developed, featuring a GaN channel between an AlN buffer and an AlN top barrier.[9–13] These structures leverage the ultrawide bandgap energy of aluminum AlN (6.2 eV), which increases the Schottky barrier height, effectively reducing gate leakage through suppressed thermionic emission and Fowler–Nordheim tunneling.[14] The large bandgap also provides robust electrical insulation in the buffer layer and a high breakdown field.[15–18] Compared to AlGaN, AlN

exhibits a stronger spontaneous polarization, resulting in a higher 2DEG density (2–3 × 10^{13} cm^2) near the AlN/GaN interface.[9,11,12] This 2DEG is tightly confined within the quantum well due to the larger conduction band offset at the GaN/AlN heterointerface, enabling precise channel modulation. However, the electron mobility of the 2DEG of AlN/GaN/AlN heterostructures is limited by a strong internal electric field within the quantum well[18] and the presence of a polarization-induced two-dimensional hole gas (2DHG).[19,20] This limited electron mobility can be enhanced by increasing the GaN quantum well thickness, which enhances electron mobility by reducing the vertical electric field, thereby decreasing scattering caused by potential fluctuations in the two-dimensional electron gas (2DEG) due to interface imperfections,[10] or by incorporating n-type compensation δ-doping in a coherently strained quantum well to remove the undesired 2DHG.[12]

In addition to the electrical benefits, AlN/GaN/AlN HEMTs offer potential thermal advantages compared to conventional AlGaN/GaN HEMTs. The higher thermal conductivity of the AlN buffer compared to GaN can enhance heat dissipation. We recently reported a 12% reduction in channel temperature for AlN/GaN/AlN HEMTs grown on a SiC substrate compared to conventional AlGaN/GaN HEMT.[13] Homoepitaxial growth of an AlN/GaN/AlN heterostructure on a bulk AlN substrate offers exceptional AlN buffer quality with ultra-low defect density, minimizing leakage and enhancing the electrical performance.[10,21] However, the thermal performance of AlN/GaN/AlN HEMTs grown on AlN substrates remains unexplored. This study investigates the self-heating behavior of two AlN/GaN/AlN HEMT structures employing homoepitaxial AlN buffer layers grown on bulk AlN substrates: (i) an AlN/strained (thin)-GaN/AlN HEMT-on-AlN, so-called AlN XHEMT,[12,13] and (ii) an AlN/relaxed (thick)-GaN/AlN HEMT-on-AlN,[10] using micro-Raman thermometry. Frequency- and time-domain thermoreflectance (FDTR and TDTR) techniques were used to characterize the phonon transport within the AlN buffer layer and across the AlN buffer/substrate interface. The thermal impact of the different device architectures was analyzed by performing 3D finite element analysis (FEA) thermal modeling.

Two types of AlN/GaN/AlN HEMT-on-AlN are compared in this study with the device schematics presented in Fig. 1. They were grown using molecular beam epitaxy (MBE) with different GaN channel thicknesses. Detailed fabrication processes and device electrical performances are described in our previous work, Ref. 22 (thin GaN channel of 20 nm), and Ref. 11 (thick GaN channel of 275 nm later confirmed by TEM), correspondingly. Both HEMT structures employ a homoepitaxially grown AlN buffer layer of 500 nm thickness on 550 μm thick AlN substrates. The first HEMT structure (AlN XHEMT) is comprised of a 20 nm coherently strained GaN channel with δ-doping to suppress the 2DHG at the bottom GaN/AlN interface, a 5.3 nm AlN barrier, a 1.5 nm GaN cap, and a 90 nm SiN passivation layer, as shown in Fig. 1(a). An alternative way to mitigate the reduction in the 2DEG mobility is to grow a thick GaN channel to reduce the vertical electric field. This configuration, shown in Fig. 1(b), includes a 275 nm relaxed GaN channel, a 3.2 nm AlN barrier, a 1.2 nm GaN cap, and a 90 nm SiN passivation layer.

To characterize the thermal conductivity (κ) of the AlN buffer layers and the thermal boundary conductance (TBC) at the AlN buffer/substrate interface, AlN films were grown on AlN substrates by MBE under identical growth conditions as the HEMT buffer layers. AlN films with thicknesses of 100, 200, 500, 1500, and 3000 nm were grown on AlN substrates to understand the role of phonon-boundary scattering effects in the homoepitaxial AlN buffer layers.

Frequency-domain thermoreflectance (FDTR) and time-domain thermoreflectance (TDTR) were used to measure the cross-plane (i.e., along the c-axis) thermal conductivity (κ_{out}) of the AlN films and the TBC at the AlN film/substrate interfaces. The FDTR system employs a continuous wave (CW) 532 nm probe laser and a 405 nm pump laser, modulated from 10 kHz to 20 MHz. The TDTR system utilizes a two-color configuration with a 514 nm pump beam and a 1028 nm probe beam (Flint FL2-12, LightConversion; 76 MHz repetition rate, ~100 fs pulse width). Detailed descriptions of both FDTR and TDTR setups are provided in previous work.[23] The measured data were fit to a multilayer heat diffusion model using Monte Carlo analysis to account for uncertainties in the assumed parameters, yielding accurate mean values and low uncertainties for the κ_{out} and TBC. For the homoepitaxial AlN films (i.e., those grown on an AlN substrate), the measured thermal responses showed no discernible difference from those of an AlN substrate, as shown in Fig. 2, indicating bulk-like thermal transport throughout the material stack. When fitting the FDTR and TDTR data assuming a finite TBC at the AlN/AlN interface, the homoepitaxial AlN films exhibited apparent κ_{out} values greater than 600 W/m K, exceeding the measured value (307.7 ± 33.4 W/m K) for the AlN substrate and theoretically calculated values (319 W/m K) for defect-free bulk AlN,[24] which is physically implausible. If the AlN film and the bulk AlN substrate are modeled as a continuous material without an interface during the data fitting processes, all the AlN films exhibit κ_{out} values consistent with the measured value (307.7 ± 33.4 W/m K) for the AlN substrate and the theoretically calculated value (319 W/m K) for defect-free bulk AlN,[24] as summarized in Table I. This indicates that homoepitaxially grown AlN films do not exhibit a thickness-dependent κ_{out}, and the thermal boundary resistance (TBR; inverse of

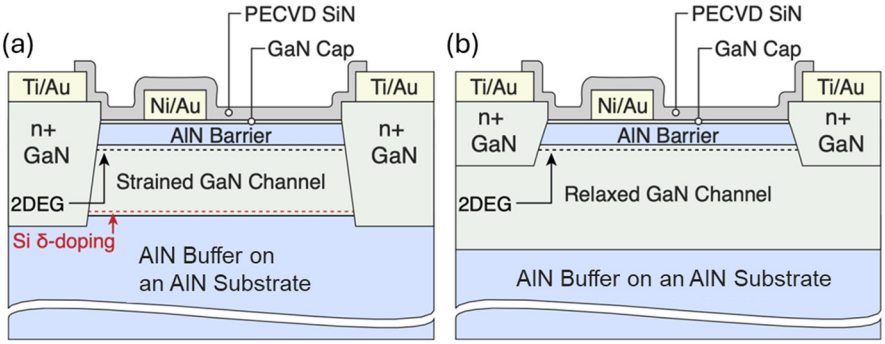

FIG. 1. Cross-sectional schematics of the AlN/GaN/AlN HEMTs on bulk AlN substrates with (a) a 20 nm pseudomorphically strained GaN channel (i.e., AlN XHEMT) and (b) a 275 nm relaxed GaN channel. Both structures employ a homoepitaxially grown 500 nm thick AlN buffer layer.

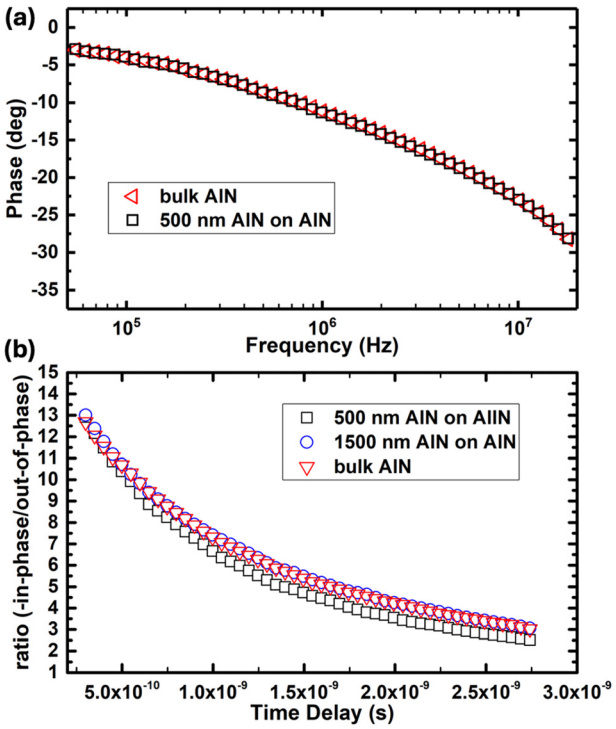

FIG. 2. Representative measured thermal responses of the AlN films by (a) FDTR and (b) TDTR. The 500 nm AlN film measured by TDTR shows a slight difference in the ratio response; however, the calculated κ_{out} values remain within the uncertainty range due to the high measurement sensitivity of TDTR, as shown in Table I.

TABLE I. The measured κ_{out} of homoepitaxial AlN films when fitting AlN on AlN as a continuous material.

AlN film thickness	FDTR	TDTR
Bulk	307.7 ± 33.4	297.9 ± 30.9
100 nm	294.2 ± 49.0	
200 nm	320.2 ± 34.2	
500 nm	311.2 ± 31.3	314.7 ± 33.9
1500 nm		293.5 ± 33.4
3000 nm	306.4 ± 67.9	

TBC) is negligible. The thermal measurement results align with prior scanning transmission electron microscopy (STEM) observations, which showed no visible growth interface between MBE-grown AlN films and the bulk AlN substrate.[25] This contrasts with previous observations of a reduced κ_{out} of heteroepitaxially grown AlN films on foreign substrates.[26–29]

Nanoparticle-assisted Raman thermometry was used to measure the channel temperature rise of the two AlN/GaN/AlN HEMTs (Fig. 1) under operation.[30] Anatase TiO_2 nanoparticles with 99.98% purity were deposited on the device surface between the gate and drain. Due to their close proximity, the measured surface temperature provides a good estimation of the 2DEG channel temperature.[31] The AlN/GaN/AlN HEMTs were operated under fully open channel conditions ($V_{GS} > 2$ V), as determined from the transfer characteristics shown in Fig. 3. The thicker GaN channel exhibits higher gate leakage current due to the thinner barrier layer and the misfit dislocations formed at the GaN/AlN interface during relaxation, which generate threading dislocations that propagate into the AlN barrier, elevating its defect density.[10,32] These defects may facilitate electron tunneling or trap-assisted conduction, thereby increasing gate leakage.[33] Controlling gate-drain leakage in AlN/GaN/AlN HEMTs can enhance breakdown voltage, as evidence shows that breakdown is primarily driven by gate-drain leakage, rather than avalanche or channel breakdown, occurring significantly below the material's intrinsic limit.[34]

Figure 4 shows the channel temperature rise of the two devices measured by Raman thermometry. The AlN XHEMT with a 20 nm strained GaN channel exhibits a significantly lower temperature rise (22% reduction) compared to the AlN/GaN/AlN HEMT-on-AlN with a thicker (275 nm) relaxed GaN channel. This trend was reproduced by a 3D finite element analysis (FEA) device thermal model accounting for the thickness-dependent κ of the GaN channel (12.3 W/m K for 20 nm GaN and 76.8 W/m K for 275 nm GaN at room temperature; calculated in Ref. 35 assuming a defect-free crystal). The temperature-dependent κ of bulk AlN was adopted from literature.[24] To mimic operation under a fully open channel condition, a uniform heat generation profile across the channel was assumed.[36] A thermal interface material (Bergquist TGP 1500R) and wafer chuck below the device die were modeled to match the experimental setup. The bottom of the wafer chuck was set at room temperature, while all other surfaces were subjected to natural convection ($h = 5$ W/m^2 K). The modeling results suggest that a thinner GaN channel is beneficial in terms of heat dissipation due to its lower thermal resistance, despite its reduced thermal conductivity. The simulation results indicate that the AlN XHEMT with a strained GaN channel exhibits a ~10% lower temperature rise under 14 W/mm whereas the experiments show a ~22% reduction in the channel temperature rise. This discrepancy is attributed to the reduction in the κ of the GaN channel due to the lattice temperature rise and the higher dislocation density in the relaxed GaN channel layer to release the misfit strain,[12] which is not captured in the calculations in Ref. 35. As reported in Ref. 10, the reciprocal space map (RSM) around the asymmetric (−105) reflection of GaN and AlN for the relaxed GaN sample confirms that the GaN layer is fully relaxed, and the peak broadening indicates significant defect generation in the channel. In contrast, the RSM of the 20-nm δ-doped GaN sample shows that the GaN layer remains coherently strained to the underlying AlN, as demonstrated in Refs. 10 and 12. It is worth noting that the Si δ-doping level (~5×10^{13} cm^{-2}) is not expected to significantly influence the κ of GaN.[35,37]

3D FEA thermal models were created for a conventional AlGaN/GaN-on-SiC HEMT and an AlN/GaN/AlN-on-SiC HEMT to further evaluate the thermal performance benefits offered by the AlN XHEMT structure. Temperature-dependent anisotropic κ of GaN,[27] AlN,[28] and 4H-SiC[27] were adopted from literature. The 4H-SiC substrate thickness was set to 550 μm (identical to that of the AlN substrate) for fair comparison. For the AlN/GaN/AlN HEMT-on-SiC, the AlN buffer was assumed to be 0.9 μm thick, similar to a device demonstrated in previous work,[27] where the κ of AlN and the TBR at the AlN/4H-SiC interface were adopted from literature.[28] The AlGaN/GaN-on-SiC HEMT had a 1.74 μm thick GaN buffer, where the κ of GaN and the TBR at the GaN/SiC interface were adopted from literature.[27] Table II

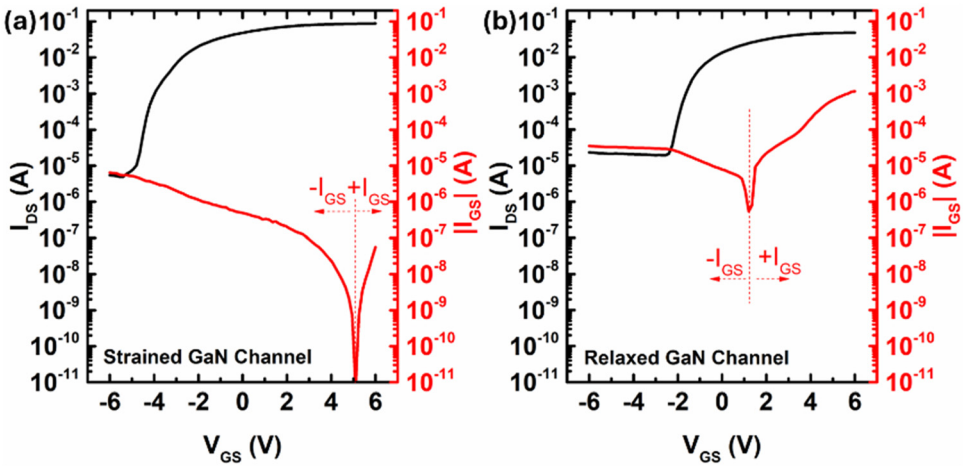

FIG. 3. Transfer characteristics and gate leakage measured at $V_{DS} = 10$ V for the AlN/GaN/AlN HEMT-on-AlN with (a) a strained GaN channel (i.e., AlN XHEMT) and (b) a relaxed GaN channel.

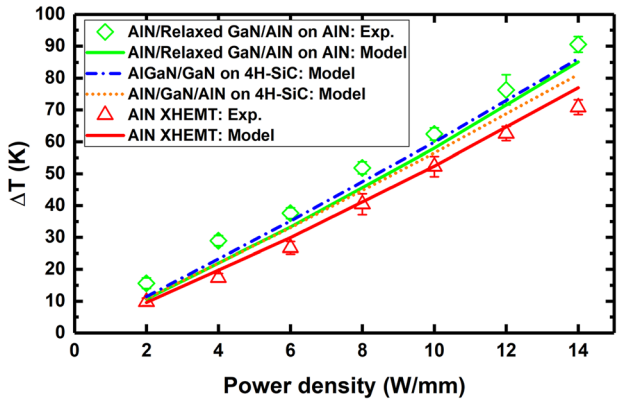

FIG. 4. Measured and simulated temperature rise of the AlN/GaN/AlN-on-AlN HEMTs with thin/strained (i.e., AlN XHEMT) and thick/relaxed GaN channels. The results are compared with the channel temperature rise of hypothetical AlGaN/GaN-on-SiC and AlN/GaN/AlN-on-SiC HEMTs via modeling.

summarizes the four device structures analyzed in Fig. 4 and relevant thermal properties.

The FEA thermal modeling results indicate that the conventional AlGaN/GaN-on-SiC HEMT exhibits a higher channel temperature than the AlN/GaN/AlN-on-SiC HEMT, similar to the findings reported in Ref. 27. This is attributed to the lower thermal conductivity of the GaN buffer layer compared to the AlN buffer. Notably, the AlN XHEMT with a strained GaN channel exhibits the lowest channel temperature rise, even lower than that of the AlN/GaN/AlN-on-SiC HEMT with a comparable GaN channel thickness (20–30 nm), despite the κ of 4H-SiC being higher than that of bulk AlN.[27,28] The superior bulk-like thermal conductivity of the homoepitaxial AlN buffer layer and the negligible TBR at the AlN buffer/substrate interface result in an enhanced device thermal performance. These results highlight the thermal benefit offered by the combined use of a high thermal conductivity homoepitaxial AlN buffer layer and a thin unrelaxed GaN channel that allows maximizing the device's thermal performance.

To preclude contributions from gate leakage current (Fig. 3) and bias-dependent self-heating effects[38,39] on the device self-heating

TABLE II. Summary of the simulated device structures, layer thicknesses, and thermal conductivities (room temperature values listed; temperature-dependent values can be found in Refs. 24, 27, and 28). κ_{in} and κ_{out} refer to the thermal conductivities along the c-axis and across the c-plane, respectively. The barrier layers are not included in the models.

	AlN/relaxed GaN/AlN on AlN	AlN XHEMT	AlGaN/GaN on 4H-SiC	AlN/GaN/AlN on 4H-SiC
Channel material and thickness	275 nm GaN	20 nm GaN	GaN—modeled as a single layer with the GaN buffer	31.5 nm GaN
GaN layer κ (W/m K)	76.8	12.3	$\kappa_{in} = 190$; $\kappa_{out} = 156$	18.5
Buffer material and thickness	0.5 μm AlN		1.74 μm GaN	0.9 μm AlN
AlN layer κ (W/m K)	313		N/A	$\kappa_{in} = 248$; $\kappa_{out} = 198$
Substrate material and thickness	550 μm AlN		550 μm 4H-SiC	
Substrate κ (W/m K)	313		$\kappa_{in} = 400$; $\kappa_{out} = 303$	

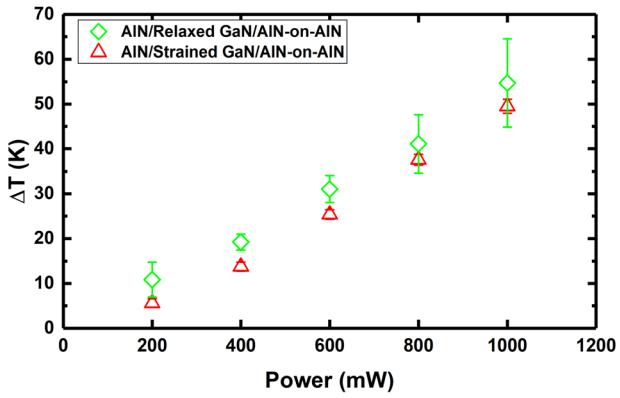

FIG. 5. The measured temperature rise of AlN/GaN/AlN-on-AlN TLM structures employing strained (i.e., AlN XHEMT) and relaxed GaN channels.

behavior, nanoparticle-assisted Raman thermometry was used to measure the channel temperature of AlN/GaN/AlN-on-AlN transmission line method (TLM) structures as shown in Fig. 5. Similar to the observations for HEMT devices, the TLM structure with a thinner strained GaN channel exhibits a lower temperature rise than the counterpart with a thicker relaxed GaN channel. These results support the aforementioned thermal benefits associated with the AlN XHEMT epitaxial structure.

A comparative analysis of the self-heating behavior of AlN/GaN/AlN HEMTs employing strained/thin (AlN XHEMT) and relaxed/thick GaN channels was performed using micro-Raman thermometry. Measurement and simulation results show that AlN/GaN/AlN-on-AlN HEMTs offer not only electrical[11,22] but also thermal benefits over conventional AlGaN/GaN-on-SiC HEMTs when employing a thin strained GaN channel. Despite SiC possessing a higher κ than AlN, the homoepitaxial AlN buffer layer exhibits a bulk AlN-like thermal conductivity due to the absence of phonon-boundary scattering at the AlN buffer/substrate interface. These findings highlight that AlN XHEMTs give promise to enhancing the performance of high-power and high-frequency radio frequency (RF) applications.

This work was partly supported by the Army Research Office under Award Nos. W911NF2220191 and W911NF-22-2-0177. This study is partly based upon work supported by the Defense Advanced Research Projects Agency (DARPA) Technologies for Heat Removal in Electronics at the Device Scale (THREADS) program under Grant No. HR0011-23-C-0135. The authors would like to thank collaborators with Raytheon—Advanced Microelectronics Solutions for their technical support. The views and conclusions contained in this document are those of the authors and should not be interpreted as representing the official policies, either expressed or implied, of the U.S. Government.

AUTHOR DECLARATIONS

Conflict of Interest

The authors have no conflicts to disclose.

Author Contributions

Yiwen Song: Data curation (lead); Formal analysis (lead); Investigation (lead); Methodology (equal); Validation (lead); Visualization (lead); Writing – original draft (lead); Writing – review & editing (lead). **Eungkyun Kim:** Formal analysis (equal); Investigation (equal); Resources (lead); Visualization (supporting); Writing – original draft (supporting); Writing – review & editing (supporting). **Jimy Encomendero:** Data curation (supporting); Formal analysis (equal); Investigation (equal); Methodology (supporting); Resources (equal). **Seokjun Kim:** Formal analysis (supporting); Investigation (supporting); Methodology (supporting); Validation (supporting). **Daniel C. Shoemaker:** Formal analysis (supporting); Investigation (supporting); Methodology (supporting); Validation (supporting). **Yu-Hsin Chen:** Formal analysis (supporting); Investigation (supporting); Resources (supporting). **Debdeep Jena:** Conceptualization (equal); Funding acquisition (equal); Project administration (equal); Resources (supporting); Supervision (equal). **Huili Grace Xing:** Conceptualization (equal); Funding acquisition (lead); Investigation (supporting); Project administration (lead); Resources (supporting); Supervision (lead); Validation (equal); Writing – original draft (supporting); Writing – review & editing (supporting). **Sukwon Choi:** Conceptualization (lead); Data curation (supporting); Formal analysis (supporting); Funding acquisition (lead); Investigation (supporting); Methodology (lead); Project administration (lead); Software (lead); Supervision (lead); Validation (equal); Writing – original draft (supporting); Writing – review & editing (supporting).

DATA AVAILABILITY

The data that support the findings of this study are available from the corresponding authors upon reasonable request.

REFERENCES

[1]R. J. Trew, G. L. Bilbro, W. Kuang, Y. Liu, and H. Yin, "Microwave AlGaN/GaN HFETs," IEEE Microwave **6**(1), 56–66 (2005).
[2]Y.-F. Wu, D. Kapolnek, J. P. Ibbetson, P. Parikh, B. P. Keller, and U. K. Mishra, "Very-high power density AlGaN/GaN HEMTs," IEEE Trans. Electron Devices **48**(3), 586–590 (2001).
[3]E. Zanoni, F. Rampazzo, C. De Santi, Z. Gao, C. Sharma, N. Modolo, G. Verzellesi, A. Chini, G. Meneghesso, and M. Meneghini, "Failure physics and reliability of GaN-based HEMTs for microwave and millimeter-wave applications: A review of consolidated data and recent results," Phys. Status Solidi A **219**(24), 2100722 (2022).
[4]H. Chandrasekar, M. J. Uren, A. Eblabla, H. Hirshy, M. A. Casbon, P. J. Tasker, K. Elgaid, and M. Kuball, "Buffer-induced current collapse in GaN HEMTs on highly resistive Si substrates," IEEE Electron Device Lett. **39**(10), 1556–1559 (2018).
[5]R. Vetury, N. Q. Zhang, S. Keller, and U. K. Mishra, "The impact of surface states on the DC and RF characteristics of AlGaN/GaN HFETs," IEEE Trans. Electron Devices **48**(3), 560–566 (2001).
[6]X. Ding, L. Song, G. Yu, Y. Cai, Y. Sun, B. Zhang, Z. Du, Z. Zeng, X. Zhang, and B. Zhang, "Gate leakage mechanisms of the AlGaN/GaN HEMT with fluorinated graphene passivation," Mater. Sci. Semicond. Process. **162**, 107502 (2023).
[7]S. Ghosh, S. Das, S. M. Dinara, A. Bag, A. Chakraborty, P. Mukhopadhyay, S. K. Jana, and D. Biswas, "OFF-state leakage and current collapse in AlGaN/GaN HEMTs: A virtual gate induced by dislocations," IEEE Trans. Electron Devices **65**(4), 1333–1339 (2018).
[8]K. Nomoto, J. Casamento, T. S. Nguyen, L. Li, H. Lee, C. Savant, A. L. Hickman, T. Maeda, J. Encomendero, V. Gund, T. Vasen, S. Afroz, D. Hannan, J. C. M. Hwang, D. Jena, and H. G. Xing, "AlScN/GaN HEMTs with 4 A/mm on-current and maximum oscillation frequency >130 GHz," Appl. Phys. Express **18**(1), 016506 (2025).
[9]A. Hickman, R. Chaudhuri, L. Li, K. Nomoto, S. J. Bader, J. C. M. Hwang, H. G. Xing, and D. Jena, "First RF power operation of AlN/GaN/AlN HEMTs

with >3 A/mm and 3 W/mm at 10 GHz," IEEE J. Electron Devices Soc. **9**, 121–124 (2021).
[10]Y.-H. Chen, J. Encomendero, C. Savant, V. Protasenko, H. G. Xing, and D. Jena, "Electron mobility enhancement by electric field engineering of AlN/GaN/AlN quantum-well HEMTs on single-crystal AlN substrates," Appl. Phys. Lett. **124**(15), 152111 (2024).
[11]E. Kim, Y.-H. Chen, J. Encomendero, D. Jena, and H. G. Xing, "AlN/GaN/AlN HEMTs on bulk AlN substrates with high drain current density >2.8 A/mm and average breakdown field >2 MV/cm," in *2024 Device Research Conference (DRC)* (IEEE, 2024), pp. 1–2.
[12]Y. H. Chen, J. Encomendero, C. Savant, V. Protasenko, H. G. Xing, and D. Jena, "High conductivity coherently strained quantum well XHEMT heterostructures on AlN substrates with delta doping," Appl. Phys. Lett. **125**(14), 142110 (2024).
[13]E. Kim, Y.-H. Chen, N. Pieczulewski, J. Encomendero, D. A. Muller, D. Jena, and H. G. Xing, "XHEMTs on ultrawide bandgap single-crystal AlN substrates," Adv. Electron. Mater. e00393 (2025).
[14]Q. Yu, C. Shi, L. Yang, H. Lu, M. Zhang, X. Zou, M. Wu, B. Hou, W. Gao, S. Wu, X. Ma, and Y. Hao, "Improved DC and RF characteristics of GaN-based double-channel HEMTs by ultra-thin AlN back barrier layer," Micromachines **15**(10), 1220 (2024).
[15]A. Yoshikawa, T. Kumabe, S. Sugiyama, M. Arai, J. Suda, and H. Amano, "Characteristics of 2DEG generated at the heterointerface of an AlN/GaN structure grown on an AlN substrate using metal organic vapor phase epitaxy," J. Appl. Phys. **137**(19), 195303 (2025).
[16]J. Lu, J.-T. Chen, M. Dahlqvist, R. Kabouche, F. Medjdoub, J. Rosen, O. Kordina, and L. Hultman, "Transmorphic epitaxial growth of AlN nucleation layers on SiC substrates for high-breakdown thin GaN transistors," Appl. Phys. Lett. **115**(22), 221601 (2019).
[17]A. L. Hickman, R. Chaudhuri, S. J. Bader, K. Nomoto, L. Li, J. C. M. Hwang, H. Grace Xing, and D. Jena, "Next generation electronics on the ultrawide-bandgap aluminum nitride platform," Semicond. Sci. Technol. **36**(4), 044001 (2021).
[18]J. Yaita, K. Fukuda, A. Yamada, T. Iwasaki, S. Nakaharai, and J. Kotani, "Improved channel electron mobility through electric field reduction in GaN quantum-well double-heterostructures," IEEE Electron Device Lett. **42**(11), 1592–1595 (2021).
[19]Z. Zhang, J. Encomendero, R. Chaudhuri, Y. Cho, V. Protasenko, K. Nomoto, K. Lee, M. Toita, H. G. Xing, and D. Jena, "Polarization-induced 2D hole gases in pseudomorphic undoped GaN/AlN heterostructures on single-crystal AlN substrates," Appl. Phys. Lett. **119**(16), 162104 (2021).
[20]R. Chaudhuri, S. J. Bader, Z. Chen, D. A. Muller, H. G. Xing, and D. Jena, "A polarization-induced 2D hole gas in undoped gallium nitride quantum wells," Science **365**(6460), 1454–1457 (2019).
[21]J. Singhal, E. Kim, A. Hickman, R. Chaudhuri, Y. Cho, H. G. Xing, and D. Jena, "AlN/AlGaN/AlN quantum well channel HEMTs," Appl. Phys. Lett. **122**(22), 222106 (2023).
[22]E. Kim, Y.-H. Chen, K. Shinohara, T.-S. Nguyen, J. Encomendero, D. Jena, and H. G. Xing, "4.2 W/mm at 10 GHz in silicon delta-doped AlN/GaN/AlN pseudomorphic HEMTs with PECVD SiN passivation," IEEE Electron Device Lett. **46**(10), 1729–1732 (2025).
[23]Y. Song, C. Perez, G. Esteves, J. S. Lundh, C. B. Saltonstall, T. E. Beechem, J. I. Yang, K. Ferri, J. E. Brown, Z. Tang, J.-P. Maria, D. W. Snyder, R. H. Olsson, B. A. Griffin, S. E. Trolier-McKinstry, B. M. Foley, and S. Choi, "Thermal conductivity of aluminum scandium nitride for 5G mobile applications and beyond," ACS Appl. Mater. Interfaces **13**, 19031 (2021).
[24]G. A. Slack, R. A. Tanzilli, R. O. Pohl, and J. W. Vandersande, "The intrinsic thermal conductivity of AlN," J. Phys. Chem. Solids **48**(7), 641–647 (1987).
[25]Y. Cho, C. S. Chang, K. Lee, M. Gong, K. Nomoto, M. Toita, L. J. Schowalter, D. A. Muller, D. Jena, and H. G. Xing, "Molecular beam homoepitaxy on bulk AlN enabled by aluminum-assisted surface cleaning," Appl. Phys. Lett. **116**(17), 172106 (2020).
[26]Y. R. Koh, Z. Cheng, A. Mamun, M. S. Bin Hoque, Z. Liu, T. Bai, K. Hussain, M. E. Liao, R. Li, J. T. Gaskins, A. Giri, J. Tomko, J. L. Braun, M. Gaevski, E. Lee, L. Yates, M. S. Goorsky, T. Luo, A. Khan, S. Graham, and P. E. Hopkins, "Bulk-like intrinsic phonon thermal conductivity of micrometer-thick AlN films," ACS Appl. Mater. Interfaces **12**(26), 29443–29450 (2020).
[27]S. Kim, E. Kim, H. Walwil, D. C. Shoemaker, J. Encomendero, M. T. DeJarld, M. B. Tahhan, E. M. Chumbes, J. R. Laroche, D. Jena, H. G. Xing, and S. Choi, "Thermal characterization and design of AlN/GaN/AlN HEMTs on foreign substrates," IEEE Electron Device Lett. **46**, 817 (2025).
[28]H. Walwil, Y. Song, D. C. Shoemaker, K. Kang, T. Mirabito, J. M. Redwing, and S. Choi, "Thermophysical property measurement of GaN/SiC, GaN/AlN, and AlN/SiC epitaxial wafers using multi-frequency/spot-size time-domain thermoreflectance," J. Appl. Phys. **137**(9), 095105 (2025).
[29]M. S. Bin Hoque, Y. R. Koh, J. L. Braun, A. Mamun, Z. Liu, K. Huynh, M. E. Liao, K. Hussain, Z. Cheng, E. R. Hoglund, D. H. Olson, J. A. Tomko, K. Aryana, R. Galib, J. T. Gaskins, M. M. M. Elahi, Z. C. Leseman, J. M. Howe, T. Luo, S. Graham, M. S. Goorsky, A. Khan, and P. E. Hopkins, "High in-plane thermal conductivity of aluminum nitride thin films," ACS Nano **15**(6), 9588–9599 (2021).
[30]J. Dallas, G. Pavlidis, B. Chatterjee, J. S. Lundh, M. Ji, J. Kim, T. Kao, T. Detchprohm, R. D. Dupuis, S. Shen, S. Graham, and S. Choi, "Thermal characterization of gallium nitride p-i-n diodes," Appl. Phys. Lett. **112**(7), 73503 (2018).
[31]S. Kim, D. C. Shoemaker, A. Karim, H. Walwil, M. T. DeJarld, M. B. Tahhan, J. Vaillancourt, E. M. Chumbes, J. R. Laroche, G. Pavlidis, S. Graham, and S. Choi, "A comparative analysis of electrical and optical thermometry techniques for AlGaN/GaN HEMTs," IEEE Trans. Electron Devices **72**(1), 162–168 (2025).
[32]P. Sohi, D. Martin, and N. Grandjean, "Critical thickness of GaN on AlN: Impact of growth temperature and dislocation density," Semicond. Sci. Technol. **32**(7), 075010 (2017).
[33]G. Meneghesso, G. Verzellesi, F. Danesin, F. Rampazzo, F. Zanon, A. Tazzoli, M. Meneghini, and E. Zanoni, "Reliability of GaN high-electron-mobility transistors: State of the art and perspectives," IEEE Trans. Device Mater. Reliab. **8**(2), 332–343 (2008).
[34]A. Hickman, R. Chaudhuri, S. J. Bader, K. Nomoto, K. Lee, H. G. Xing, and D. Jena, "High breakdown voltage in RF AlN/GaN/AlN quantum well HEMTs," IEEE Electron Device Lett. **40**(8), 1293–1296 (2019).
[35]T. E. Beechem, A. E. McDonald, E. J. Fuller, A. A. Talin, C. M. Rost, J.-P. Maria, J. T. Gaskins, P. E. Hopkins, and A. A. Allerman, "Size dictated thermal conductivity of GaN," J. Appl. Phys. **120**(9), 95104 (2016).
[36]R. Pearson, B. Chatterjee, S. Kim, S. Graham, A. Rattner, and S. Choi, "Guidelines for reduced-order thermal modeling of multifinger GaN HEMTs," J. Electron. Packag. **142**(2), 021012 (2020).
[37]Y. Song, J. S. Lundh, W. Wang, J. H. Leach, D. Eichfeld, A. Krishnan, C. Perez, D. Ji, T. Borman, K. Ferri, J.-P. Maria, S. Chowdhury, J.-H. Ryou, B. M. Foley, and S. Choi, "The doping dependence of the thermal conductivity of bulk gallium nitride substrates," J. Electron. Packag. **142**(4), 041112 (2020).
[38]S. Choi, E. R. Heller, D. Dorsey, R. Vetury, and S. Graham, "The impact of bias conditions on self-heating in AlGaN/GaN HEMTs," IEEE Trans. Electron Devices **60**(1), 159–162 (2013).
[39]B. Chatterjee, C. Dundar, T. E. Beechem, E. Heller, D. Kendig, H. Kim, N. Donmezer, and S. Choi, "Nanoscale electro-thermal interactions in AlGaN/GaN high electron mobility transistors," J. Appl. Phys. **127**(4), 44502 (2020).